Journal Name

ARTICLE

Tailoring the self-assembly of a tripeptide for the formation of antimicrobial surfaces

Received 00th January 20xx,
Accepted 00th January 20xx

DOI: 10.1039/x0xx00000x

www.rsc.org/

Sivan Nir[a], David Zanuy[b]*, Tal Zada[a], Omer Agazani[a], Carlos Aleman[b], Deborah E. Shalev[c,d]* and Meital Reches[a]*

The accumulation of bacteria on surfaces is currently one of the greatest concerns for the supply of proper health, water and energy. Here, we describe the mechanism by which a single peptide forms two pH-dependent supramolecular particles that resist bacterial contamination. By using NMR and molecular dynamics (MD), we determined the structures of the peptide monomers and showed the forces directing the self-assembly of each structure under different conditions. These peptide assemblies change the characteristics of bare glass and confer it with the ability to prevent biofilm formation. Furthermore, they can adsorb and release active compounds as demonstrated with an anticancer drug, antibiotic and enzyme. This synergism and the detailed understanding of the processes are necessary for developing new sterile surfaces for health-care systems, water purification devices, food packaging or any environment that suffers from biocontamination.

Introduction

Biofouling is a process in which organisms and biomolecules accumulate on a surface.[1, 2] It initiates with the adsorption of biomolecules, such as proteins and polysaccharides, which form a conditioning film. Bacteria attach to this film creating a well-defined bacterial network, termed "biofilm".[3] The biofilm subsequently produces metabolites that promote the attachment of higher organisms. This process eventually results in a thick layer of foulants.[1, 2, 4]

The biofilm is a multicellular community of bacteria that relies on intercellular exchange of chemical signals, called quorum sensing. The coordinated biofilm becomes pathogenic and can resist antibiotic treatment.[1, 5, 6] Biofilm on medical devices and implants can lead to severe infection, which can cause death.[7] In the US alone, the American Centers for Disease Control and Prevention (CDC) reported that healthcare-associated infections account for an estimated 1.7 million infections and 100,000 deaths annually.[8]

One proposed solution to prevent biofilm formation on medical devices is to incorporate antibiotics in a releasing system.[9] For example, loading catheters with a leaching system that releases antibiotics in a slow and controlled manner, preventing bacterial accumulation and infection.[10] These systems are not limited to antibiotics – they can also release metal nanoparticles such as silver and copper.[11] Natural compounds such as plants extracts, marine metabolites and enzymes can also be used in the battle against bacterial strains that are resistant to antibiotics.[12-15] Another technique is to anchor biocides to the device itself.[16, 17] The anchored biocides either eradicate the bacteria that come into contact with the surface or produce chemical species, such as reactive oxygen species (ROS), that obliterate bacteria near the surface.[18]

Anti-biofouling approaches and materials target the establishment of the conditioning film. These materials alter the surface energy, either physically or chemically making the adsorption process less favorable.[1, 2, 4] For example, this can be done by designing the topography of a surface to prevent fouling.[19-22] This approach was inspired by natural surfaces such as shark skin or lotus leaves.[23] Alternatively, different coatings hinder the interactions of biomolecules and organisms with solid surfaces.[24-28]

We have designed a tripeptide that can self-assemble into a coating with anti-biofouling properties in organic solvents.[29] The peptide sequence, DOPA-Phe(4F)-Phe(4F)-OMe, contains three elements that enable its (i) adsorption onto any substrate, [27, 30-33] (ii) self-assembly into a film, [34-41] and (iii) anti-biofouling property.[1, 4] The tripeptide is relatively simple to synthesize and it self-assembles spontaneously on the substrate without the need of any pre- or post-treatment. The assembly is not limited to a specific substrate and can be applied to metals, oxides, and polymers.

The coating precludes the first step of fouling by preventing biomolecules from attaching to the surface,[4] and it can also significantly reduce the amount of bacteria on the surface.[29]

[a] Institute of Chemistry and The Center for Nanoscience and Nanotechnology, The Hebrew University of Jerusalem, Jerusalem, 91904 Israel.
[b] Department of Chemical Engineering and Barcelona Research Center in Multiscale Science and Engineering, Universitat Politècnica de Catalunya, C/ Eduard Maristany, 10-14, 08019, Barcelona, Spain.
[c] The Wolfson Centre for Applied Structural Biology, The Hebrew University of Jerusalem, Jerusalem, 91904 Israel.
[d] Department of Pharmaceutical Engineering, Azrieli College of Engineering, Jerusalem 9103501, Israel

Electronic Supplementary Information (ESI) available: experimental data, figures and tables. See DOI: 10.1039/x0xx00000x

This paper shows that the self-assembly of this tripeptide is not limited only to organic solvents, but can also occur in aqueous solutions. These solutions are greener and more appealing for producing environmentally friendly materials.[42] Once transferring peptides into water based media, their solubility and tendency to self-assemble can be easily modulated by changing the salinity or the pH of the solution.[43]

In aqueous solutions, under acidic and mildly basic conditions the peptide self-assembles into spherical particles that differ by size and morphology. Since the building block of these particles is an anti-biofouling peptide, we speculated that the particles would exhibit anti-biofouling properties. In addition, as the peptide consists of DOPA moiety, it should be able to adhere to surfaces and modify them. This modification would also alter the topography of the surface and therefore might improve the anti-biofouling performance of the surface compared to substrate coated with the nanometric peptide layer from the organic solvents.

Furthermore, we present the particles potential as controlled release systems and show that the surface antimicrobial efficiency is improved by this ability.

Results and discussion

Particles characterization

To initiate self-assembly of the tripeptide, the peptide was dissolved in either an acidic (1 M HCl, pH=1) or basic (Tris buffer, 10 mM, pH=8.5) solution. Scanning Electron Microscopy (SEM) analysis revealed that the peptide immediately self-assembled into different structures under acidic or basic conditions. Interestingly, within the time-scale of the process, we could not detect any indication of catechol oxidation involvement in the self-assembly of the latter condition.

In acidic medium, the peptide self-assembled into smooth spheres with an average diameter of 2.0±0.4 µm (Fig. 1a). In basic medium, the peptide self-assembled into porous spiky spheres with an average diameter of 26±3 µm (Fig. 1b).

Interesting trends in structure and size could be observed upon changing pH. SEM analysis revealed that lowering the acidity of the solution resulted in smaller spheres. Figure S1 (ESI‡) presents the changes in spheres from pH 1 to 6. The spheres became increasingly smaller until no spheres could be detected. Upon increasing the pH from 6.5 to 9, the spikes enlarged so they were maximized at the range of pH 7.5-8.5. Above pH=9, the spiky spheres became denser and less spiky (Fig. S2, ESI‡). This may be attributed to the sensitivity of DOPA to pH.[27] These findings suggest that the physical properties of the spheres (*i.e.* porosity, size) and their appearance could be fine-tuned by controlling the pH values of the solution and that the optimal pH value for self-assembly was 8-8.5.

The ionic strength of the solution affected the self-assembly process. SEM analyses of assemblies from Tris buffer concentrations ranging from 1 mM to 20 mM showed that at a concentration of 1 mM the majority of the surface was covered with amorphous aggregates. The few spiky spheres that were detected were denser than those obtained in 10 mM (Fig. S3, ESI‡). At 5 mM Tris, spiky spheres appeared in small clusters of only a few assemblies with amorphous aggregates among the ordered structures, whereas at 10 mM Tris they appeared in large clusters that were free from aggregates. At higher concentrations, such as 15 mM and 20 mM, the amorphous aggregates were again dominant and the few spheres that formed were denser and larger than at 10 mM. Accordingly, 10 mM Tris was chosen as optimal self-assembly conditions.

Fourier Transform Infrared Spectroscopy analysis (FTIR) was used to analyse the secondary structures of the peptide assemblies. The spectrum of the smooth spheres had a single wide peak at 1631 cm^{-1} which corresponds to a β-sheet structure.[44] Deconvolution analysis resulted in a predominant peak at 1635 cm^{-1}, accompanied by additional small peak at 1664 cm^{-1} that also correlate β-structures. Another lower peak which significantly overlapped its neighbouring peaks was observed at 1648 cm^{-1}. This peak correlated unordered structures (random). In addition, deconvoluted spectrum revealed that the peak broadening could have been intensified by the overlapping of the amide I region with side chains bands and -NH_3^+ asymmetric bending between 1570 to 1620 cm^{-1}.[44]

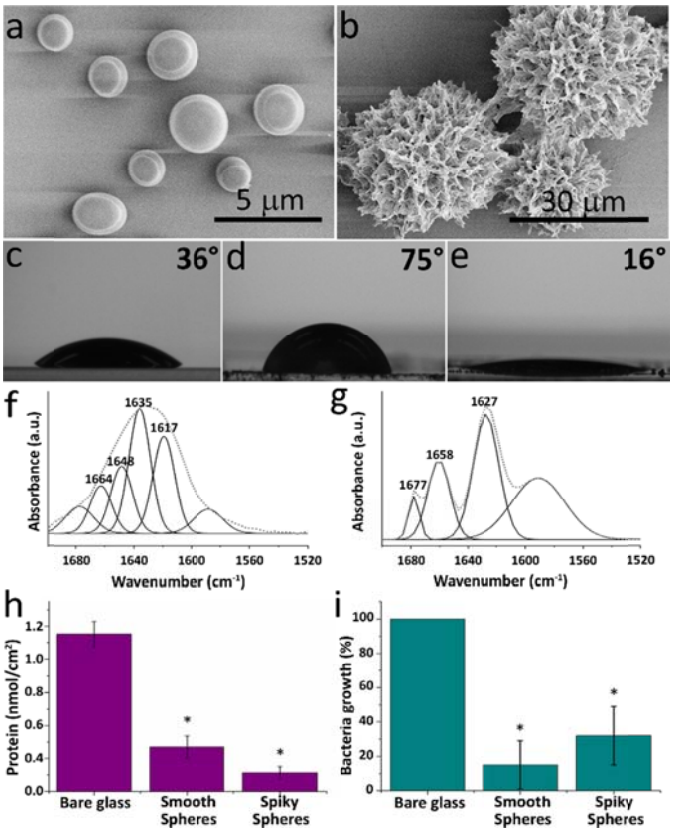

Figure 1. Structural and functional characterization of the peptide assemblies. (a-b) Scanning electron micrographs of (a) smooth spheres formed under acidic conditions, 1 M HCl and (b) spiky spheres formed under basic conditions, 10 mM tris buffer, pH=8.5. (c-e) Water contact angles of (c) a bare glass slide, (d) a glass slide coated with the smooth spheres, and (e) a glass slide coated with the spiky spheres. Amide-I region of de-convoluted FT-IR spectra of the (f) smooth sphere and (g) spiky sphere assemblies. (h) The

adsorbed amounts of BSA on the smooth sphere-assembly and spiky sphere-assembly modified surfaces. (i) The normalized amount of *E.coli* adsorbed onto the modified surfaces. Data were analysed by t-test. **P*-value < 0.05 compared to control.

Considering the original spectra obtained by the FTIR, the deconvoluted peaks intensities, broadness and overlapping regions, we concluded that the prevailing conformation in the smooth spheres is that of β-sheet.

The spectrum of spiky spheres showed three distinctive peaks at 1627, 1658 and 1677 cm^{-1} (Fig. 1f-g). Compared to the smooth spheres spectrum, the peaks obtained were more resolved and easily detected prior to deconvolution. These peaks suggest a structure that contain high percentage of β-sheet, but may also combine α-helical secondary structures,[44] correlating the more complex microstructures formed under these conditions.

Particles-coated surfaces

The assemblies-coated surfaces showed new microtopography. Surfaces were coated with the peptide assemblies (1mg/mL) by allowing the peptide to self-assemble and drop-casting the peptide solution (150 µL) onto clean glass slides. After the samples dried in air, they were thoroughly washed with triple distilled water (TDW) to remove remains of acidic/basic solution and excess and non-adhered peptide. Finally, the surfaces were dried under nitrogen.

The degree of coverage by the structures was assessed using ImageJ[45] and MATLAB. Analysis of SEM micrographs showed that the smooth spheres coated 78% of the surface while spiky spheres coated only 40% of it. This is due to the tendency of the spiky spheres to aggregate, leaving larger gaps on the surface, whereas smooth spheres remain unconnected. Lower concentrations gave the same structures, but resulted in a poor coverage of the surfaces. At higher concentrations or when applied a few times on the surface, the smooth spheres merged and no improvement in coverage was evaluated for them nor for the spiky spheres (Fig. S4, ESI‡).

Understanding how the coated-surfaces interact with water is important as both hydrophobicity and hydrophilicity play a major role in efficient anti-biofouling materials.[1, 4]

The water contact angle of the surfaces exhibited an increase from 36˚ for bare glass to 75˚ for smooth sphere-coated glass. The increased contact angle indicates an increase in hydrophobicity which likely stems from the hydrophobic features of the peptide and the new topography of the surface. On the other hand, surfaces coated with spiky spheres showed a decrease in contact angle to 16˚ (Fig. 1c-e), indicating a hydrophilic surface. In fact, when placed on the surface, the water droplet was immediately adsorbed by it. This behaviour can be explained by the porosity of the spiky spheres; upon dehydration of the surface when modified with spiky spheres, water evaporate, leaving empty pores that allow the penetration of water.

Anti-biofouling properties of the particles modified surfaces

Surfaces decorated with peptide assemblies showed resistance to protein adsorption. Bare and peptide-coated glass slides were incubated in a solution of Bovine Serum Albumin (BSA) and the adsorbed amounts of protein were quantified. The amount of protein adsorbed on the bare glass was substantially higher than the amount of protein adsorbed on the peptide-coated glass (Fig. 1h). The smooth spheres, formed in acidic medium, reduced the amount of adsorbed protein from 1.9 $nmol/cm^2$ to 0.5 $nmol/cm^2$. The spiky spheres formed in basic medium reduced the amount of adsorbed protein from 1.9 $nmol/cm^2$ to 0.28 $nmol/cm^2$.

Previous reports have shown that BSA has a higher tendency to adsorb onto hydrophobic surfaces than hydrophilic surfaces, but also that it undergoes denaturation and spatial rearrangement while adsorbing onto surfaces. Its spatial orientation depends on the surface area in which it can spread.[46] Since the spiky spheres form non-smooth surfaces with complex topography, they may be more effective against the protein relative to the smooth spheres.

Bare and peptide-modified surfaces were incubated with *Escherichia coli* in nutrient medium overnight to allow the adsorption of bacteria and the formation of biofilms on the surfaces. After incubation, the bacteria were removed from the surfaces by sonication, diluted 10-fold, plated and the colony-forming units (CFUs) were counted. The surfaces coated with the different peptide assemblies exhibited anti-biofouling properties where the number of colonies counted from these samples was lower than that from the bare glass. The spiky spheres reduced the bacterial growth by 68% and the smooth spheres reduced it by 85% (Fig. 1i). Similar results were also obtained for longer incubation times (up to 72 h, data not shown).

Understanding the parameters governing the self-assembly

NMR characterization of monomers. The structures of the monomers under different conditions were determined by Nuclear Magnetic Resonance Spectroscopy (NMR) to study the characteristics that lead to different morphologies of the supramolecular structures. Spectra were acquired under acidic (10 mM HCl, pH=1), salt (10 mM NaCl, pH=7) and basic (10 mM tris buffer, pH=8.5) conditions. The basic sample did not yield any informative resonance peaks due to broadening out under these conditions. Therefore, further analysis under the basic conditions was performed on the low-energy structure simulated by molecular dynamics and compared to the structures obtained by NMR.

Spectra acquired under identical conditions were assigned according to Wultrich[47] and resulted in well-defined ensembles (Fig. S5-S6 and tables S1-S3, ESI‡).

The three representative structures from each condition differed from each other. The low-energy representative ensemble derived under acidic conditions had backbone and heavy atom RMSD values of 0.004 Å and 0.616 Å, respectively. This ensemble was stabilized by varying interactions that included cation-π,[48] NH-π[49] and CH-π[50] intramolecular interactions (Fig. S7, ESI‡). Due to the flexible conformation of the acidic monomer, the side chains and backbone are available to form intermolecular interactions with either the solvent or other peptide molecules.

The low-energy ensemble under salt conditions, comprising the 10 lowest energy conformations, had a backbone RMSD of 0.001 Å and heavy atom RMSD of 0.608 Å. Similar stabilizing interactions were found in all members of the calculated ensemble: An intramolecular hydrogen bond; a weak cation-π interaction and a parallel-displaced π-π stacking (Fig. S7, ESI‡.[48, 51] The unusual stability of the monomers, evident in their remarkably low RMSD values, results in a restrained conformation that favours a monomeric state over self-assembly, explaining why no supramolecular structures are formed under salt conditions (Fig. S8, ESI‡).

The monomer orientation under basic condition was obtained from molecular dynamics and showed no stabilizing intramolecular interactions. The peptide backbone was extended – exposing its polar residues, *i.e.*, carbonyls and amides, and the side groups pointed outwards. This conformation would allow the polar substituents on the rings, *i.e.* the hydroxyl and fluorine atoms, to form stabilizing hydrogen bonds with the solvent (Fig. S9, ESI‡). This conformation also permits intramolecular interactions between one monomer to another.

A full columbic potential calculation performed on the representative structure from each condition (acidic, salt, basic) showed the potential distribution over the monomer molecules. These surface potentials could indicate how molecules would interact at short-ranges (Van der Waals distances) (Fig. S7, ESI‡).

Self-assembly mechanism. Considering the data obtained from the NMR analysis, we could deduce the different modes of self-assembly. Under acidic conditions, restricted by the conformational space, geometry and charge, positive Phe2 of one monomer may interact with the negative pocket of the adjacent molecule (Video S1 and S2, ESI‡). This can give rise to π-π stacking among the aromatic rings of both monomers (Fig. 2a) and may enable intermolecular hydrogen bond formation between the Phe2 carbonyl of one monomer and the Phe3 amide of the next. Additional monomers would approach in the same manner, resulting in a directed growth that yields dense spherical structures. Recent reports have mentioned the interactions of hydronium ions with aromatic systems: The binding enthalpy of multi-layered aromatic complexes was shown to increase by establishing cation-π interactions with H_3O^+ ions.[52] The acidic environment encouraged the assembly process, as opposed to the salt conditions system where sodium ions, that are known to stabilize biological complexes via cation-π interactions,[53] shielded the aromatic rings from additional intermolecular interactions.

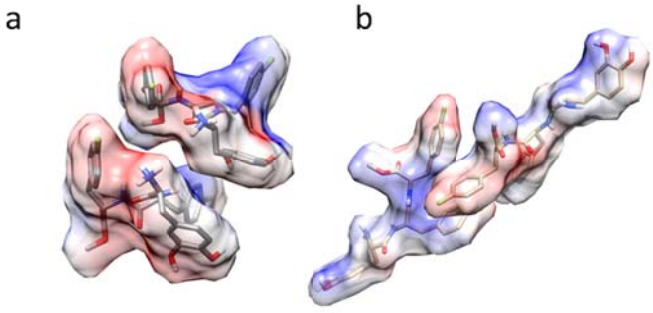

Figure 2. Representation of the self-assembly process from the representative monomer under (a) acidic conditions and under (b) basic conditions.

Under basic conditions, the monomer seems to self-assemble in a different manner: Negatively charged region of the Phe3 may approach another monomer in between the Phe3 amide and the positive region of the Phe2 (Fig. 2b and videos S3, ESI‡). Further adjustments may result in π-π interactions, hydrogen bonds (NH···F) or NH-π interactions. Since the peptide backbone is extended, additional monomers could be attracted to other functional sites. This open conformation enables various geometries of π-π interactions (*e.g.* T-shape, Y-shape, edge-to-face).[51]

The interlayer properties of the π-π interactions may change the orientation of subsequent monomer binding – resulting in spiky spheres.

Molecular dynamics simulations. The self-assembly process was simulated by molecular dynamics (Table S4, ESI‡). A complete survey of non-bonding interactions, performed on each studied molecular model (Table 1), showed the influence of the different environments on the spatial arrangement of the peptide and the ability of the peptide chains to remain consistently associated. Under acidic conditions, the inter-chain distances resembled those of beta-sheets as also seen from the IR results.[34] After 20 ns of simulation, 60% of the initial hydrogen bonds among the main chains were preserved and supported a packing which was dense (Figure 3a).

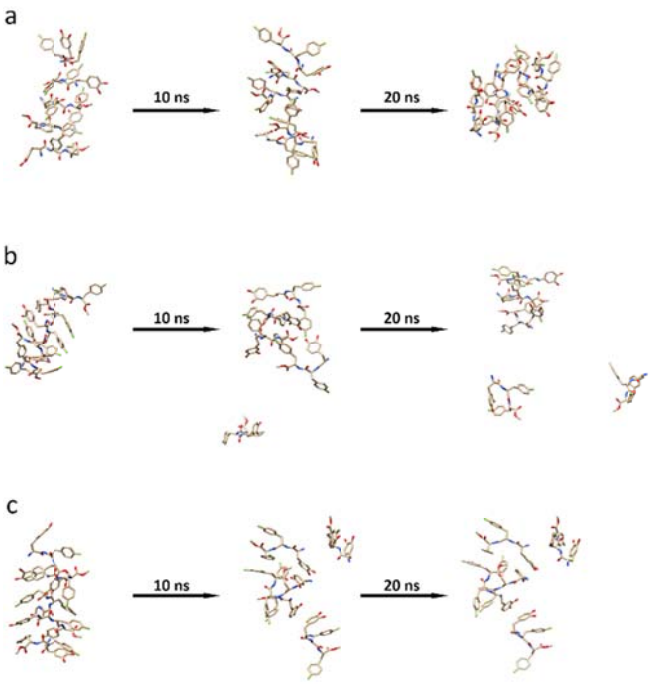

Figure 3. Representation of the time-dependent evolution of peptide assemblies by molecular dynamics under (a) acidic, (b) salt

and (c) basic conditions. Heteroatoms coloured according to CPK convention: blue – nitrogen, red – oxygen and green – fluorine. Non-polar hydrogen atoms were removed for clarity.

The basic conditions seemed to facilitate a global disorganization which favoured the formation of hydrogen bonds among chains that initially were apart. Despite this quick loss of regular organization,

Table 1. Summary of the number of inter- and intra-strand interactions within each assembly.

		Hydrogen Bonds			π-π stacking		π-π stacking	N-H-π
Time	Conditions	β-strand[a]	Nt-Ct[b]	Other[c]	β-strand[d]	Other[e]	Intra-strand	
First ns	Acidic	7	2	1	7	2	Chains I & V	
	Salt	5	2	0	5	6	Chain V	
	Basic	0	1	3	8	2	Chain I	
Last ns	Acidic	5	3	3	4	7	Chain II	
	Salt	2	1	1	4	3	Chain I	Chain I
	Basic	0	0	4	1	4	Chains IV & V	Chains II & V

a Hydrogen bonds between amide groups of neighbouring strands from an initial β-strand arrangement. The maximal number of possible amide-amide hydrogen bonds with five strands arranged in antiparallel fashion is 8. b Hydrogen bonds between the terminal ester carbonyl and amino terminal group. c Other inter-strand hydrogen bonds. d π-π stacking interactions between adjacent molecules in a β-sheet. e Other inter-strand π-π stacking interactions. Data averaged over the initial and final ns of the simulation. An interaction is computed as present if it is detected in at least 90% of the studied consecutive frames.

some intermolecular π-stacking interactions were preserved, allowing the peptide strands to stay associated. At the end of the simulation, distances among the chains were larger than under acidic conditions (Table S5, ESI‡). This might allow hydrogen bonding of free backbone amides with water or guest molecules. The interactions among the side chains, which involved hydrogen bonds and π-π stacking, could support the supramolecular structure (Fig. 3c). The molecular dynamic simulations under salt conditions correlated the experimental results: At the beginning of the run the peptide monomers grouped together, but within 10 ns they started to disassemble. The assembly continued to break apart at 20 ns explaining why no supramolecular structures were observed at the end of the process (Fig. 3b and Table 1).Though the processes simulated by the MD is depicted by only five monomers they can nicely represent nucleation sites from which the self-assembly initiates. More monomers might exhibit the same behaviour.

The final assemblies simulated by the MD simulations resembled those suggested by the NMR-derived mechanism. The monomers interact with each other via hydrogen bonds of the backbones amides and carbonyls, and these interactions encourage intra-strand π-π stacking between the same side groups. These interactions are spread along the peptide molecule so eventually the chains are closely associate with each other, what leads to a dense packing. More peptide monomers would interact in the same manner, increasing the core volume of the assembly.

On the other hand, the assembly from basic conditions does not involve any backbone-backbone interactions and mostly supported by π-π stacking and hydrogen bonds among different side groups. This leads to a sparse packing that is not directed, does not involve the full length of the peptide molecule and as a result is held by specific focal points. Additional monomers would assemble by forming new points, increasing the space occupied by the assembly.

Anti-biofouling mechanism. The structural data supports a plausible mechanism that sheds light on the adsorption of spheres to surfaces and their ability to prevent adsorption of proteins and bacteria: During the coating process, water evaporates and fewer molecules

are available to interact with the catechol moieties of the peptide. This leads to strong binding of the catechols to the surface.[54] Once the coated surfaces are placed in an aqueous environment, the components of the assembly that face the water are hydrated, forming microsolvated catechol-H_2O complexes that interact with water molecule clusters.[55] This hydration neutralizes the adhesiveness of the unoccupied catechols. The increased volume of surface hydration enhances anti-biofouling by forming a steric barrier.[24] The anti-adhesive features of the fluorine atoms that point towards the solvent[6] further prevent the process of fouling.

Peptide particles capability of entrapping and releasing active compounds

The ability of the assemblies to adsorb or encapsulate active compounds can be used to improve their antimicrobial properties. Doxorubicin was used as a model to show incorporation into assemblies by fluorescence spectroscopy. Peptides were added to either acidic or basic media containing additional doxorubicin (50 μg/mL) and the fluorescence intensity at 590 nm before and after the addition was measured. The intensity of the dye markedly decreased when the peptide was added (Fig. S11, ESI‡), presumably owing to its encapsulation or adsorption to the peptide assemblies.

The solution was drop-casted onto a glass cover slip and dried under ambient conditions. The glass was then rinsed with water to remove the excess dye and non-adsorbed peptide. Fluorescence microscope showed a fully stained surface for glass slides casted

with doxorubicin, whereas the slides casted with peptide and drug exhibited distinct fluorescent spheres. The drug specifically adsorbed onto the peptide assemblies without affecting their structure (Fig. 4a-c).

To detect release of the drug, peptide assemblies were incubated with the drug overnight. During the incubation, the peptide assemblies precipitated (Fig. S12, ESI‡), were subsequently washed, collected and placed in a dialysis membrane. The fluorescence intensity of the buffer outside the membrane was sampled for 9 days. Doxorubicin concentration increased over time in both the smooth spheres and spiky spheres samples. However, the release from the smooth spheres formed in acidic medium was faster and reached equilibrium after two days (Fig. 4d,f). In the case of the spiky spheres sample, a controlled release pattern was observed. After 9 days, the spiky spheres were still coloured indicating that not all of the dye had been released, suggesting the peptide assemblies can act as an active leaching surface by releasing antibacterial compounds (Fig. 4e,g) .

The internal structures of the assemblies were examined by Focused Ion Beam Scanning Electron Microscopy (FIB-SEM). 3D images of the smooth spheres formed under acidic conditions, revealed a packed structure (Fig. S13 a,c, ESI‡).

The spiky spheres on the other hand, collapsed when the ion beam was applied (Fig. S13 b,d, ESI‡), suggesting the interior arrangement of these spheres was similar to the exterior high degree of porosity, which was responsible for the structural collapse. These findings indicated that the drug was adsorbed onto the surface of the smooth spheres, while encapsulated in the spiky spheres. These results along with the molecular dynamics simulations (Fig. 3) lead us to conclude that the different release patterns arise from the morphology of the assemblies and not their size. Doxorubicin is rapidly released from the surface of the smooth spheres, whereas the voids in the porous spiky spheres act as reservoirs, resulting in prolonged release.

Improved antimicrobial/anti-biofouling performance by co-assembly

The inherent anti-biofouling properties of the assemblies were combined with antimicrobial features from compounds such as antibiotics and hydrogen peroxide.

Co-assembly with gentamicin. Glass slides coated with peptide assemblies formed in the presence of the antibiotic gentamicin were incubated in buffer overnight and then, 10 µL were spotted onto agar inoculated with *E.coli.* After allowing the bacteria to grow, plates were examined for zones of inhibition. Clear zones were observed where the buffer media were applied and not in plates spotted with buffer media drops taken at t=0 or drops taken from bare glass slides. The average diameter of inhibition from the antibiotic released from the smooth spheres was 0.84±0.07 cm, and from the spiky spheres it was 0.94±0.06 cm (Fig. S14, ESI‡). These diameters correlate to concentrations of 85 µg/mL and 130 µg/mL respectively. No inhibition zones were developed at shorter incubation times, probably due to the lower gentamicin amounts leached to that point. The results for zones of inhibition correlate with the results obtained for doxorubicin. The release plots presented in figure 4f-g show intensities that resemble each other at the first few hours – the burst in release from the smooth spheres appears only after 24 hours. Therefore, in the duration of this assay, the zones of inhibition radius should be similar.

Co-assembly with Glucose Oxidase. Glucose Oxidase (GOx) is an enzyme that oxidizes glucose into gluconolactone and hydrogen peroxide. Hydrogen peroxide has a general mechanism of disrupting bacterial cell walls, leading to bacterial death.[56, 57] The enzyme was incorporated into the peptide assemblies to improve the antibacterial activity of the surfaces. Since the enzyme is sensitive to pH and would denature under the acidic conditions, it was co-assembled with the peptide only under mild basic conditions that resulted in spiky spheres. The concentration of GOx co-assembled with the peptide was optimized in a way that self-assembly could still result in spiky spheres. Bare glass slides and modified glass slides were incubated in the inoculums of *E.coli* for one hour. After incubation, the bacteria were removed from the surface, plated and CFUs were counted. Substrates coated with spiky spheres showed a ~70% reduction of bacteria relative to non-coated glass; Glass slides coated with GOx alone showed a slightly reduced amount of bacteria, apparently due to residual enzyme molecules that formed non-specific interactions with the surface; and the surfaces with combined peptide and GOx exhibited superior activity.

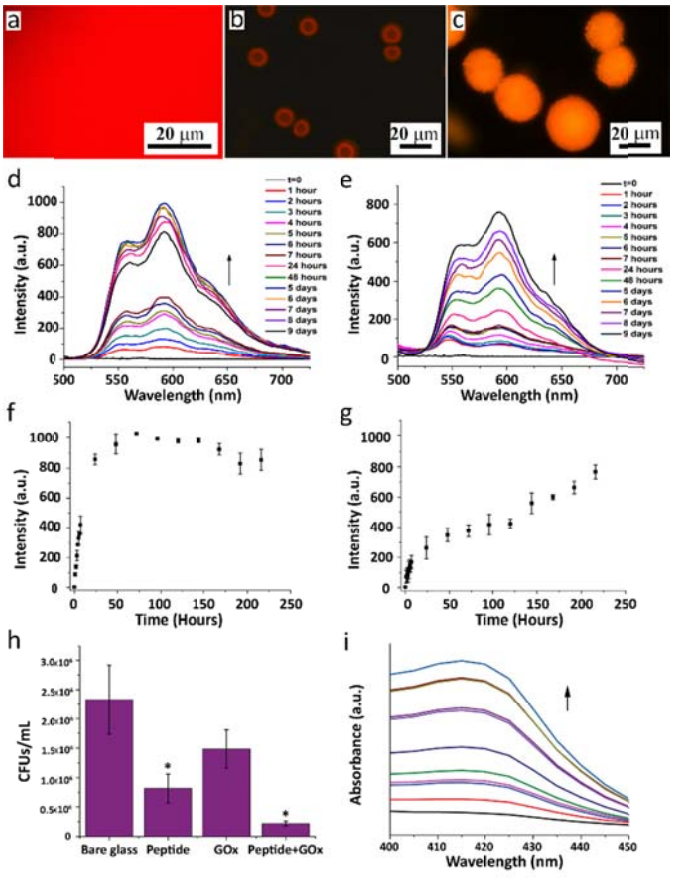

Figure 4. Release of active molecules from the peptide assemblies. (a-c) Fluorescence microscopy micrographs of (a) doxorubicin on bare glass, (b) peptide smooth spheres under acidic conditions with doxorubicin, and (c) peptide spiky spheres under basic conditions with doxorubicin; Fluorescence intensity increase upon release of doxorubicin from (d, h) smooth spheres and (e, g) spiky spheres. Fluorescence intensity at 590 nm as a function of time for doxorubicin released from (f) smooth spheres and (g) spiky spheres. Bars represent standard deviation. (h)The number of CFUs resulting from surfaces modified with either the peptide assemblies, the enzyme GOx, or a combination of the assemblies and GOx; Data were analysed by t-test. **P-value* < 0.05 compared to control. (i) Absorption spectrum of $ABTS^{\bullet-}$ at 414 nm, from t=0 min (black) to t=60 min (dark cyan), indicating of H_2O_2 release.

The number of bacteria decreased by an order of magnitude, from 2.3×10^6 CFUs/mL to 2.1×10^5 CFUs/mL which corresponds to a log reduction (Fig. 4h). Combining the assembly properties with the GOx activity improved the overall ability of the surface to resist fouling.

The amount of GOx encapsulated in the spiky spheres was quantified using the enzyme labelled with fluorescent $Atto_{590}$-NHS to enhance sensitivity of detection. The concentration of free GOx was measured in solution before and after adding the peptide. The amount of GOx in the assemblies was 64 µg per mg of peptide (Fig. S15, ESI‡), which correlated to 16 enzymatic units.

The oxidation of $ABTS^{2-}$ by Horseradish Peroxidase (HRP) was measured to verify release of hydrogen peroxide from the spheres. HRP oxidizes $ABTS^{2-}$ to $ABTS^{\bullet-}$ in the presence of hydrogen peroxide: The oxidized product absorbs at 414 nm.[58] Figure 4i presents the increase in absorption at 414 nm of the oxidized product. The absorption of $ABTS^{2-}$ at 340 nm decreased with time (Fig. S16, ESI‡). Within one hour of exposing bacteria to the surfaces, the concentration of hydrogen peroxide was 5.2×10^{-6} M.

Conclusions

The DOPA-Phe(4F)-Phe(4F)-OMe tripeptide has been shown to coat surfaces and prevent biofouling.29 We showed that this peptide can self-assemble into two distinctive structures depending on the pH of the solution. The process was followed from the monomeric structures of the peptides under acidic, basic and neutral conditions; through the dynamic self-assembly to supramolecular structures. Acidic conditions gave smooth, solid spheres which adsorbed active compounds on their surfaces and released them rapidly. Basic conditions resulted in spiky spheres with large surface areas and porous interiors which could encapsulate large amounts of active compounds and release them in an extended manner.

We proposed a mechanism, by which assemblies adhere to surfaces and exhibit anti-biofouling properties due to their fluorinated moieties and hydration barrier. The inherent anti-biofouling properties of the assemblies were enhanced by antibiotics and a catalytic enzyme and this system can be easily extended to incorporate other antimicrobial agents such as quorum-sensing quenchers and metal nanoparticles.

The ability to design and regulate the anti-biofouling and antimicrobial properties of surfaces, along with understanding the processes that control these functionalities, are crucial for fabricating new devices that withstand bacterial contamination and thereby are resistant towards fouling. These devices can be useful in any system that could be compromised by the accumulation of biomass, such as the health-care system, water transport facilities and the food industry.

Conflicts of interest

"There are no conflicts to declare".

Acknowledgements

M.R. acknowledges the support of the Water Authority and the Focal Technology Area (FTA) of the Israeli Initiative for Nanoscience, S.N. acknowledges the support of the Water Authority.
C.A. and D.Z. acknowledge MINECO/FEDER (MAT2015-69367-R) for financial support. C.A. is grateful to ICREA Academia program for excellence in research.
The authors acknowledge Mr. T. Duanis-assaf for his help with FTIR deconvolution.

Notes and references

1. 1. S. Nir and M. Reches, *Curr. Opin. Biotechnol.* 2016, **39**, 48-55.
2. C. M. Kirschner and A. B. Brennan, in *Annual Review of Materials Research, Vol 42*, Annual Reviews, Palo Alto, 2012, vol. 42, pp. 211-229.
3. L. C. Gomes, L. N. Silva, M. Simoes, L. F. Melo and F. J. Mergulhao, *J.Biomed.Mater. Res., Part A*, 2015, **103**, 1414-1423.
4. M. Lejars, A. Margaillan and C. Bressy, *Chem. Rev.*, 2012, **112**, 4347-4390.
5. B. K. Bharati and D. Chatterji, *Curr. Sci.*, 2013, **105**, 643-656.
6. N. Amara, B. P. Krom, G. F. Kaufmann and M. M. Meijler, *Chem. Rev.*, 2011, **111**, 195-208.
7. R. O. Darouiche, *N. Engl. J. Med.*, 2004, **350**, 1422-1429.
8. R. M. Klevens, J. R. Edwards, C. L. Richards, Jr., T. C. Horan, R. P. Gaynes, D. A. Pollock and D. M. Cardo, *Public Health Rep.*, 2007, **122**, 160-166.
9. H. F. Chuang, R. C. Smith and P. T. Hammond, *Biomacromolecules*, 2008, **9**, 1660-1668.
10. H. J. Busscher, H. C. van der Mei, G. Subbiahdoss, P. C. Jutte, J. J. A. M. van den Dungen, S. A. J. Zaat, M. J. Schultz and D. W. Grainger, *Sci.Transl.Med.*, 2012, **4**, 153rv110-153rv110.
11. G. Yeroslavsky, R. Lavi, A. Alishaev and S. Rahimipour, *Langmuir : the ACS J .Surf. Colloid.*, 2016, **32**, 5201-5212.
12. N. Fusetani, *Nat.Prod.Rep*, 2011, **28**, 400-410.
13. H. Bar-Rogovsky, A. Hugenmatter and D. S. Tawfik, *J.Biol. Chem.*, 2013, **288**, 23914-23927.
14. T. Stern, E. Zelinger and Z. Hayouka, *Chem. Commun.* (Cambridge, England), 2016, **52**, 7102-7105.

15. C. Gajadeera, M. J. Willby, K. D. Green, P. Shaul, M. Fridman, S. Garneau-Tsodikova, J. E. Posey and O. V. Tsodikov, *J. Antibiot.*, 2015, **68**, 153-157.
16. A. J. Martin-Rodriguez, J. M. F. Babarro, F. Lahoz, M. Sanson, V. S. Martin, M. Norte and J. J. Fernandez, *Plos One*, 2015, **10**.
17. R. T. C. Cleophas, M. Riool, S. A. J. Zaat, P. J. L. M. Quaedflieg, J. A. W. Kruijtzer and R. M. J. Liskamp, *Abstr. Pap .Am. Chem. S.*, 2012, **244**.
18. L.-E. Shi, Z.-H. Li, W. Zheng, Y.-F. Zhao, Y.-F. Jin and Z.-X. Tang, *Food.Addit. Contam. Part A,* 2014, **31**, 173-186.
19. J. Yue, P. Zhao, J. Y. Gerasimov, M. van de Lagemaat, A. Grotenhuis, M. Rustema-Abbing, H. C. van der Mei, H. J. Busscher, A. Herrmann and Y. Ren, *Adv. Funct. Mater.*, 2015, **25**, 6756-6767.
20. M. L. Carman, T. G. Estes, A. W. Feinberg, J. F. Schumacher, W. Wilkerson, L. H. Wilson, M. E. Callow, J. A. Callow and A. B. Brennan, *Biofouling*, 2006, **22**, 11-21.
21. S. Pechook, K. Sudakov, I. Polishchuk, I. Ostrov, V. Zakin, B. Pokroy and M. Shemesh, *J. Mater. Chem. B*, 2015, **3**, 1371-1378.
22. A. K. Epstein, T.-S. Wong, R. A. Belisle, E. M. Boggs and J. Aizenberg, *Proc. Natl. Acad. Sci. USA*, 2012, **109**, 13182-13187.
23. G. D. Bixler and B. Bhushan, Crit. Rev. *Solid State Mater. Sci.*, 2015, **40**, 1-37.
24. X. J. Khoo, P. Hamilton, G. A. O'Toole, B. D. Snyder, D. J. Kenan and M. W. Grinstaff, *J.Am. Chem. Soc.*, 2009, **131**, 10992-10997.
25. C. M. Grozea and G. C. Walker, *Soft Matter*, 2009, **5**, 4088-4100.
26. N. Zhao, Z. Wang, C. Cai, H. Shen, F. Liang, D. Wang, C. Wang, T. Zhu, J. Guo, Y. Wang, X. Liu, C. Duan, H. Wang, Y. Mao, X. Jia, H. Dong, X. Zhang and J. Xu, *Adv. Mater.* , 2014, **26**, 6994-7017.
27. H. Lee, S. M. Dellatore, W. M. Miller and P. B. Messersmith, *Science*, 2007, **318**, 426-430.
28. R. Konradi, C. Acikgoz and M. Textor, Macromol. *Rapid. Commun.*, 2012, **33**, 1663-1676.
29. S. Maity, S. Nir, T. Zada and M. Reches, *Chem. Commun.*, 2014, **50**, 11154-11157.
30. J. H. Waite and M. L. Tanzer, *Science*, 1981, **212**, 1038-1040.
31. T. Gillich, E. M. Benetti, E. Rakhmatullina, R. Konradi, W. Li, A. Zhang, A. D. Schlueter and M. Textor, *J.Am. Chem. Soc.*, 2011, **133**, 10940-10950.
32. J. Sedo, J. Saiz-Poseu, F. Busque and D. Ruiz-Molina, *Adv. Mater.*, 2013, **25**, 653-701.
33. P. R. Spycher, H. Hall, V. Vogel and E. Reimhult, *Biomater. Sci.* , 2015, **3**, 94-102.
34. M. J. Krysmann, V. Castelletto, A. Kelarakis, I. W. Hamley, R. A. Hule and D. J. Pochan, *Biochem.*, 2008, **47**, 4597-4605.
35. X. Y. Gao and H. Matsui, *Adv. Mater.*, 2005, **17**, 2037-2050.
36. C. Tang, A. M. Smith, R. F. Collins, R. V. Ulijn and A. Saiani, *Langmuir*, 2009, **25**, 9447-9453.
37. R. F. Silva, D. R. Araujo, E. R. Silva, R. A. Ando and W. A. Alves, *Langmuir*, 2013, **29**, 10205-10212.
38. S. G. Zhang, *Nat. Biotechnol.*, 2003, **21**, 1171-1178.
39. M. Reches and E. Gazit, *Science*, 2003, **300**, 625-627.
40. S. Yuran, Y. Razvag and M. Reches, *ACS Nano*, 2012, **6**, 9559-9566.
41. S. Maity, S. Nir and M. Reches, *J. Mater. Chem. B.*, 2014, **2**, 2583-2591.
42. M. O. Simon and C. J. Li, *Chem. Soc. Rev.*, 2012, **41**, 1415-1427.
43. X. Zhao, F. Pan and J. R. Lu, *Prog. Nat. Sci.*, 2008, **18**, 653-660.
44. H. Susi and D. M. Byler, *Methods Enzymol.*, 1986, **130**, 290-311.
45. C. A. Schneider, W. S. Rasband and K. W. Eliceiri, *Nat. Methods,* 2012, **9**, 671-675.
46. J. Kim and G. A. Somorjai, *J. Am. Chem. Soc.*, 2003, **125**, 3150-3158.
47. K. Wüthrich, *NMR of Proteins and Nucleic Acids*, John Wiley & Sons, New York, 1986.
48. M. S. Marshall, R. P. Steele, K. S. Thanthiriwatte and C. D. Sherrill, *J. Phys. Chem. A*, 2009, **113**, 13628-13632.
49. S. K. Burley and G. A. Petsko, *FEBS Lett.*, 1986, **203**, 139-143.
50. K. Sundararajan, K. Sankaran, K. S. Viswanathan, A. D. Kulkarni and S. R. Gadre, *J. Phys. Chem.A*, 2002, **106**, 1504-1510.
51. C. R. Martinez and B. L. Iverson, *Chem.Sci.*, 2012, **3**, 2191-2201.
52. M. A. Montes-Moran, J. A. Menendez, E. Fuente and D. Suarez, *J. Phys. Chem. B*, 1998, **102**, 5595-5601.
53. J. P. Gallivan and D. A. Dougherty, *Proc. Natl. Acad. Sci. USA*, 1999, **96**, 9459-9464.
54. P. Das and M. Reches, *Nanoscale*, 2016, **8**, 15309-15316.
55. B. Gomez-Zaleta, R. Gomez-Balderas and J. Hernandez-Trujillo, *Phys. Chem.Chem. Phys.*, 2010, **12**, 4783-4790.
56. M. R. Guascito, D. Chirizzi, C. Malitesta, L. Giotta, D. Mastrogiacomo, L. Valli and L. Stabili, *Biopolymers*, 2014, **101**, 461-470.
57. G. Amitai, J. Andersen, S. Wargo, G. Asche, J. Chir, R. Koepsel and A. J. Russell, *Biomaterials*, 2009, **30**, 6522-6529.
58. S. Lilienthal, Z. Shpilt, F. Wang, R. Orbach and I. Willner, *ACS Appl. Mater.Interfaces*, 2015, **7**, 8923-8931.